Talanta 156-157 (2016) 225–231

Contents lists available at ScienceDirect

Talanta

journal homepage: www.elsevier.com/locate/talanta

# Plasmonically amplified bioassay – Total internal reflection fluorescence *vs.* epifluorescence geometry

Simone Hageneder [a], Martin Bauch [a,b], Jakub Dostalek [a,*]

[a] Biosensor Technologies, AIT-Austrian Institute of Technology, Muthgasse 11, 1190 Vienna, Austria
[b] Energy Department, AIT-Austrian Institute of Technology, Giefinggasse 2, 1210 Vienna, Austria

ARTICLE INFO

*Article history:*
Received 11 January 2016
Received in revised form
4 May 2016
Accepted 8 May 2016
Available online 11 May 2016

*Keywords:*
Biosensor
Surface plasmon resonance
Fluorescence
Bioassay
Grating
Total internal reflection fluorescence
Epifluorescence

ABSTRACT

This paper investigates plasmonic amplification in two commonly used optical configurations for fluorescence readout of bioassays – epifluorescence (EPF) and total internal reflection fluorescence (TIRF). The plasmonic amplification in the EPF configuration was implemented by using crossed gold diffraction grating and Kretschmann geometry of attenuated total reflection method (ATR) was employed in the TIRF configuration. Identical assay, surface architecture for analyte capture, and optics for the excitation, collection and detection of emitted fluorescence light intensity were used in both TIRF and EPF configurations. Simulations predict that the crossed gold diffraction grating (EPF) can amplify the fluorescence signal by a factor of $10^2$ by the combination of surface plasmon-enhanced excitation and directional surface plasmon-coupled emission in the red part of spectrum. This factor is about order of magnitude higher than that predicted for the Kretschmann geometry (TIRF) which only took advantage of the surface plasmon-enhanced excitation. When applied for the readout of sandwich interleukin 6 (IL-6) immunoassay, the plasmonically amplified EPF geometry designed for Alexa Fluor 647 labels offered 4-times higher fluorescence signal intensity compared to TIRF. Interestingly, both geometries allowed reaching the same detection limit of 0.4 pM despite of the difference in the fluorescence signal enhancement. This is attributed to inherently lower background of fluorescence signal for TIRF geometry compared to that for EPF which compensates for the weaker fluorescence signal enhancement. The analysis of the inflammation biomarker IL-6 in serum at medically relevant concentrations and the utilization of plasmonic amplification for the fluorescence measurement of kinetics of surface affinity reactions are demonstrated for both EPF and TIRF readout.



## 1. Introduction

Fluorescence spectroscopy represents an established method for detection of chemical and biological species and it supports a wide range of optical readers for protein and oligonucleotide assays [1,2]. In order to advance the sensitivity of such assays and to use them for rapid analysis of trace amounts of biomolecules, we witnessed increasing research efforts in near-field optics and particularly plasmonics [3]. Plasmonics concerns the manipulating of light at sub-wavelength scale by its coupling to surface plasmons (SPs) originating from collective oscillations of charge density at surface of metallic films and metallic nanoparticles. Plasmonic nanostructures have found their applications in amplification of signal in optical spectroscopy including surface enhanced Raman spectroscopy (SERS), surface enhanced infrared spectroscopy (SEIRA), and plasmon-enhanced fluorescence (PEF) spectroscopy [4–6]. In fluorescence spectroscopy-based detection of molecular analytes, a sandwich assay format with *e.g.* secondary antibody labeled with a fluorophore is typically used. These fluorophores are coupled with the confined field of SPs to increase the excitation rate at their absorption wavelength and improve extraction of fluorescence light at their emission wavelength from the sensor surface. In addition, the coupling with SPs mediates the emitter radiation rate which can improve its quantum yield $\eta$ (particularly for fluorophores with intrinsically low $\eta$). Due to the strongly confined field profile of SPs, the coupling occurs in close vicinity to the sensor surface which allows selectively amplifying the signal originating from the specific binding without increasing background.

Up to now, numerous implementations of PEF that utilize the excitation of SPs propagating along continuous metallic films, as well as localized SPs supported by metallic nanoparticles, were pursued [7–9]. Either the attenuated total reflection (ATR) method with Kretschmann configuration or diffraction on periodically corrugated metallic surface was employed for the coupling of propagating SPs with far field optical waves. Kretschmann

* Corresponding author.
*E-mail address:* jakub.dostalek@ait.ac.at (J. Dostalek).

http://dx.doi.org/10.1016/j.talanta.2016.05.023
0039-9140/

geometry was utilized for fluorescence immunoassays with SP-enhanced excitation and collection of fluorescence light in the beginning of nineties of the last century [10]. This approach was later re-introduced and served for the combined SP-enhanced fluorescence with refractometric surface plasmon resonance (SPR) sensing [11]. The directional SP-coupled emission was exploited based on the reverse Kretschmann configuration by using prism elements [8] or concentric diffractive structures [12]. The Kretschmann geometry allows for the implementation of plasmonic amplification into fluorescence readers that resemble total internal reflection fluorescence (TIRF) configuration. Diffraction gratings offer an alternative means for the coupling of far field with SPs and can be used in epifluorescence (EPF) devices. The coupling with propagating SPs was demonstrated to amplify the fluorescence signal by a factor up to $10^2$ with respect to configurations where the fluorophores are present in homogenous environment and emit isotropically into the far field [13,14].

This paper concerns the implementation of plasmonic amplification for *in situ* readout of fluorescence assays. It describes TIRF and EPF configurations for the detection of fluorescence signal through a microfluidic device which requires using low numerical aperture lens optics for its collection. We compare the readout of a realistic assay by using TIRF and EPF geometries that utilize the SP-assisted excitation and extraction of emitted fluorescence light. For each readout configuration key characteristics of the assay are determined and improvements and limitations associated with the coupling with SPs are discussed. As a target analyte cytokine interleukin 6 (IL-6) is selected as it plays important role in regulating inflammatory and immune responses and is aberrantly expressed in diseases including cancer [15,16]. Therefore we witness a need for the timely and accurate monitoring of this protein in clinical research, disease diagnosis as well as in therapy. Enzyme-linked immunosorbent assay (ELISA) is arguably a golden standard method for the highly specific analysis of IL-6 at concentrations below pg/mL [17]. Research is pursued in areas such as point-of-care diagnostic sensors in order to simplify the IL-6 analysis which currently requires laboratory conditions and can only be used by trained personnel. In this field, a range of techniques is investigated including electro- or electrochemical sensors [18,19] as well as surface acoustic wave sensors or fluorescence biosensors [20–22].

## 2. Materials and methods

### 2.1. Materials

Polydimethylsiloxane elastomer (PDMS) Sylgard 184 was obtained from Dow Corning (USA) and the UV-curable polymer Amonil MMS 10 was from AMO GmbH (Germany). The carboxylate (SPT 0014A6) and PEG-dithiols (SPT 0013) were purchased from SensoPath Technologies (USA). EDC [1-Ethyl-3-(3-dimethylaminopropyl) carbodiimide] and NHS (N-hydroxysuccinimide) were obtained from Thermo Scientific (Germany). Ethanolamine (1 M in water) was purchased from Sigma Aldrich (Austria) and adjusted to pH 8.5 with HCl. 10 mM acetate buffer (ACT) with pH 4.0 was prepared from sodium acetate and acetic acid and the pH was adjusted by HCl and NaOH. The used antibody pair of purified monoclonal rat anti-IL-6 (clone MQ2-13A5; product number 13-7068) and biotinylated monoclonal rat anti-human IL-6 (clone MQ2-39C3; product number 14-7069), as well as human IL-6 (product number 34-8069) were obtained from eBioscience (Austria). A reference capture antibody against p53 from Sigma Aldrich was used. Streptavidin Alexa Fluor 647 conjugate (product number S32357; in average 3 fluorophores per molecule) was purchased from Life Technologies (USA). Phosphate buffered saline (PBS) and Tween 20 were obtained from Sigma Aldrich (Austria) and biotin-free albumin fraction V was from Roth, Germany. Standard serum samples with concentrations of human IL-6 of 8.4, 131 and 437 pg/mL were acquired from Randox (UK).

### 2.2. Sensor chip preparation

For plasmonically amplified measurements relying on TIRF geometry, 2 nm thick chromium adhesion promoting layer and 45–50 nm thick gold film were subsequently deposited on a glass substrate by using vacuum thermal evaporation (HHV AUTO 306 from HHV LTD). For the EPF experiments, a 4 nm thick chromium adhesion promoting layer and a 100 nm thick gold film were prepared by the same means on a substrate with periodically corrugated surface. These substrates were structured by soft lithography as we described before [13]. Briefly, a master crossed-grating structure was fabricated by using laser interference lithography and transferred to a PDMS working stamp. This stamp was used for the preparation of multiple replicas to an UV-curable polymer Amonil MMS 10 that was spin-coated on a BK7 glass substrate. The corrugation profile $h(x,y)$ of copied rectangular crossed grating surface with deposited gold film can be described by using Cartesian coordinates ($x$ and $y$ axis are in the plane of the substrate) as the function $h(x,y)=\alpha(\sin[(2\pi/\Lambda)x]+\sin[(2\pi/\Lambda)y])+\beta(\sin[(2\pi/\Lambda)x]+\sin[(2\pi/\Lambda)y])^2$, where $\Lambda$ is the period and $\alpha$ and $\beta$ are modulation amplitudes. $\alpha$ describes the linear and $\beta$ the nonlinear response of the UV sensitive photoresist used in interference lithography for master fabrication. The parameters of the crossed grating profile used further are $\Lambda=434$ nm, $\alpha=4$ nm and $\beta=2.5$ nm as determined by atomic force microscopy (AFM). The formula of the surface profile allows for implementation of the crossed grating geometry in the simulation method, as later mentioned. It is worth of noting that corrugations with low values of the non-linear parameter $\beta$ exhibit weak Bragg scattering of propagating SPs which simplifies design of the grating for efficient amplification of fluorescence signal.

### 2.3. Optical setup

The used optical setup for TIRF and EPF readout of a sandwich IL-6 immunoassay is presented in Fig. 1. Identical light-source, sensor chip biointerface architecture, flow cell, and a module for

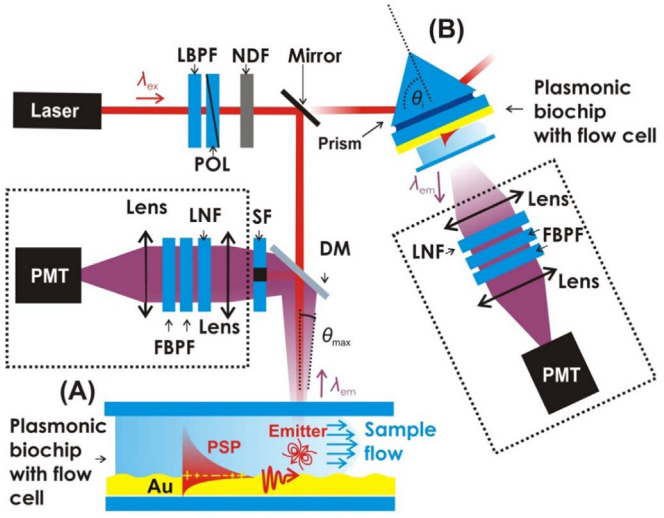


**Fig. 1.** Optical setup of used for assay with *in situ* plasmonically enhanced fluorescence readout relying on (A) epifluorescence geometry and (B) total internal reflection fluorescence.

collecting the fluorescence light to a detector were used in both configurations. In the TIRF geometry, a beam emitted from a HeNe laser passed through a laser band-pass filter (FL632.8-10 from Thorlabs), a polarizer, and a neutral density filter (1%). TM polarized beam at the wavelength $\lambda_{ex}=633$ nm with the intensity of 1.5 μW was coupled to a 90° prism coupler made of LASFN9 glass. To the prism base, a sensor chip with flat surface coated by 45 nm gold film was optically matched by using immersion oil (from Cargille Inc., USA). Against the surface of the sensor chip, a flow-cell was clamped in order to contain aqueous liquid samples. A flow cell with a volume of 1.5 μL was made from a thin PDMS gasket and sealed by a transparent fused silica glass substrate. Into the silica substrate, inlet and outlet ports were drilled and connected by tubing (Tygon R3607, 0.13 mm) to a peristaltic pump. The angle of incidence $\theta$ of the excitation beam hitting the gold sensor surface was adjusted at the reflectivity minimum in order to assure the resonant coupling to SPs at the interface with an aqueous sample. The enhanced field intensity of SPs excited randomly oriented fluorophore labels at the distance $f$ from the gold sensor surface. The emitted fluorescence light at $\lambda_{em}=670$ nm was collected by a module with a lens (focal length 50 mm and numerical aperture of $NA=0.2$, LB1471 from Thorlabs, UK) and passed through a set of filters consisting of a notch filter (XNF-632.8-25.0M from CVI Melles Griot, Germany) that was used to block the excitation wavelength $\lambda_{ex}$ and two bandpass filters (FB670-10 from Thorlabs and 670FS10-25 from Andover Corporation Optical Filter) with the transmission window centered at the $\lambda=670$ nm and spectral width of about 10 nm. The fluorescence beam was focused at the input of a photomultiplier (H6240-01, Hamamatsu, Japan) that was connected to a counter (53131A from Agilent, USA). The output from the counter was recorded in counts per second (cps) by using software Wasplas developed at the Max Planck Institute for Polymer Research in Mainz (Germany). In the setup with EPF readout, an excitation beam was reflected by a dichroic mirror (XF2087 660DRLP from Omega Optical) towards the sensor chip with clamped transparent flow-cell on its top. By using neutral density filters, the intensity of the excitation beam was set to be the same as in the TIRF geometry. The gold sensor chip surface was corrugated by a grating designed for the first order diffraction coupling of fluorescence light to SPs by a normally incident beam at $\lambda_{ex}$. The dichroic mirror (XF2087 660DRLP from Omega Optical, USA) was tilted by 45° where it is highly reflective at the wavelength $\lambda_{ex}$ and transparent at the emission wavelength of $\lambda_{em}=670$ nm. The fluorescence light emitted from the sensor surface passed through the dichroic mirror and it was collected and delivered to the identical detector and as in the TIRF geometry. Before the lens, the fluorescence beam travelled through a spatial filter that blocked the partially reflected excitation beam at the wavelength $\lambda_{ex}$ (blocking the light emitted to cone with polar angle $\theta<1°$).

### 2.4. Surface modification

The gold surface of flat and corrugated sensor chips was modified by a mixed thiol self-assembled monolayer (SAM). Immediately after the deposition of the gold layer, the sensor chips were immersed in a 1 mM solution of PEG and COOH-dithiols that were dissolved in ethanol at 1:9 M ratio and incubated overnight in order to form a SAM. Afterwards, the surface was copiously rinsed with ethanol, dried with a stream of nitrogen, and stored under argon atmosphere. Prior to an assay experiment, the sensor chip was mounted to the EPF or TIRF optical setup and a flow cell was clamped on its top. The sensor chip surface was modified with capture (anti-IL-6) or reference (anti-p53) antibodies *in situ* by using amine coupling. Carboxyl groups on the surface were reacted with aqueous solution containing 21 mg/mL NHS and 75 mg/mL EDC for 15 min. Then the surface was rinsed by ACT buffer with pH=4 and the cAb dissolved in the same ACT buffer at concentration of 50 μg/mL was flowed over the surface for 20 min until saturation was reached (observed *in situ* with surface plasmon resonance – SPR). Finally, unreacted active ester groups were passivated by a 20 min flow of 1 M ethanolamine, pH 8.5.

### 2.5. IL-6 sandwich immunoassay

All assay experiments were performed in PBS working buffer with 0.05% Tween 20 and 1 mg/mL albumin fraction V. Samples for calibration of the sensor were prepared by spiking working buffer with purified IL-6 at concentrations 42 fM to 4.2 nM. Serum samples were diluted 10-fold by working buffer. The used sandwich assay is illustrated in Fig. 2(A). Prior to the assay, the sensor surface was rinsed with working buffer for 5 min in order to establish a baseline in the sensor response $F$. Then, the analyzed sample was flowed through the sensor for 10 min followed by 5 min rinsing with working buffer. Afterwards, biotinylated anti-IL-6 antibody was flowed at 1 μg/mL for 10 min. After subsequent 5 min rinsing with working buffer, Alexa Fluor 647 – labeled streptavidin at concentration of 2 μg/mL was circulated though the sensor for 10 min and its surface was rinsed with a working buffer for additional 5 min. The sensor signal increase $\Delta F$ after the

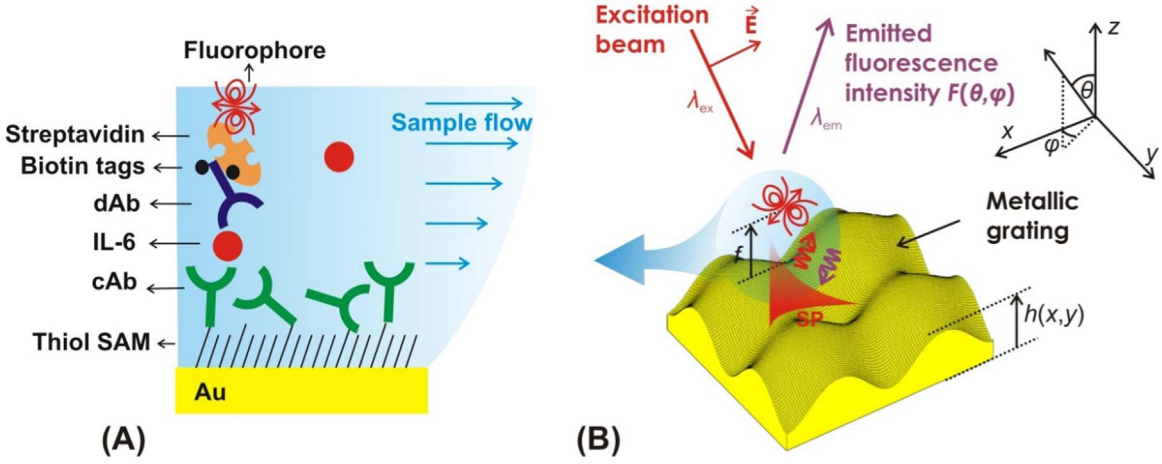


**Fig. 2.** (A) Biointerface architecture (identical for flat and corrugated gold surfaces) with a schematic of sandwich immunoassay for detection of IL-6. (B) Geometry of the fluorescence excitation and emission on a crossed grating surface with epifluorescence readout.

binding of SA was determined as a sensor response. All samples and reagents were flowed through the sensor at the flow rate of 15 μL/min.

### 2.6. Simulations

Optical simulations were carried out to investigate the angular distribution of emitted fluorescence light mediated by SPs at the gold surface. The out-coupling of SPs generated by fluorescence emission to optical waves propagating to the far field occurs when they are phase-matched along the metallic surface. In simulations, the far field emission was expressed as the intensity dependence on azimuthal $\phi$ and polar $\theta$ angles defined in Fig. 2(B). For the Kretschmann geometry, plane waves propagating in the glass prism are coupled to SPs when the following condition is fulfilled:

$$\frac{2\pi}{\lambda} n_p \sin(\theta_i) = \mathrm{Re}\left\{\frac{2\pi}{\lambda}\sqrt{\frac{n_m^2 n_s^2}{n_m^2 + n_s^2}}\right\}, \quad (1)$$

where $\lambda$ is the wavelength, $n_p$ is the refractive index of prism, $\theta_i$ is the angle of incidence taken in the prism, $n_m$ is the refractive index of gold, and $n_s$ is the refractive index of an aqueous sample. The diffraction coupling to SPs by a light beam hitting the crossed gold grating surface through an aqueous sample occurs when:

$$\left[\frac{2\pi}{\lambda}\sin(\theta)\cos(\phi) + p\frac{2\pi}{\Lambda}\right]^2 + \left[\frac{2\pi}{\lambda}\sin(\theta)\sin(\phi) + q\frac{2\pi}{\Lambda}\right]^2 = \left[\mathrm{Re}\left\{\frac{2\pi}{\lambda}\sqrt{\frac{n_m^2 n_s^2}{n_m^2 + n_s^2}}\right\}\right]^2, \quad (2)$$

where $p$ and $q$ are diffraction orders. The polar angle $\theta$ and the azimuthal angle $\phi$ are assumed in air outside the flow cell. The simulation of the interaction of SPs with optical waves at $\lambda_{ex}$ and a dipole emitting radiation at $\lambda_{em}$ were pursued by using finite difference time domain (FDTD) simulations implemented in the package FDTD Solutions from Lumerical Solutions Inc. (Canada). The fluorescence enhancement *EF* can be evaluated from simulation results by the following equation:

$$EF = \frac{\left\langle \left|\vec{E}(\lambda_{ex})\cdot\vec{\mu}_{ab}\right|^2 \eta\cdot CE \right\rangle}{\left\langle \left|\vec{E}_0(\lambda_{ex})\cdot\vec{\mu}_{ab}\right|^2 \eta_0\cdot CE_0 \right\rangle}, \quad (3)$$

where the brackets ⟨ ⟩ indicate an averaging over different positions and orientations of the fluorophore (represented in the simulation by the absorption dipole $\vec{\mu}_{ab}$ and emission dipole $\vec{\mu}_{em}$). $\vec{E}$ and $\vec{E}_0$ states for the simulated electric field intensity in the presence and absence of the plasmonic structure. Similarly, $\eta_0$ and $\eta$ are the emitter quantum yields with and without the metallic surface. Collection efficiency that is mediated by surface plasmon-coupled emission is described as *CE* and $CE_0$ is the reference value. The near field distribution of electric field intensity at the gold surface $|E|^2$ was normalized with that of the incident wave $|E_0|^2$. For angular distribution of emitted light, a dipole emitter radiating at $\lambda_{em}$ was placed in vicinity to the gold surface. The surface plasmon-mediated angular distribution of emission intensity was normalized with the total emitted intensity. Thus obtained emission probability $F(\theta,\phi)$ was calculated for randomly oriented dipole at the distance from the gold surface of $f=20$ nm and the *CE* was obtained by its integration over polar and azimuthal angles falling to the $NA=0.2$. The distance $f$ was estimated from the typical size of used molecules in the sandwich assay sketched in Fig. 2(A). Obtained emission characteristics were averaged over the unit cell area $\Lambda \times \Lambda$.

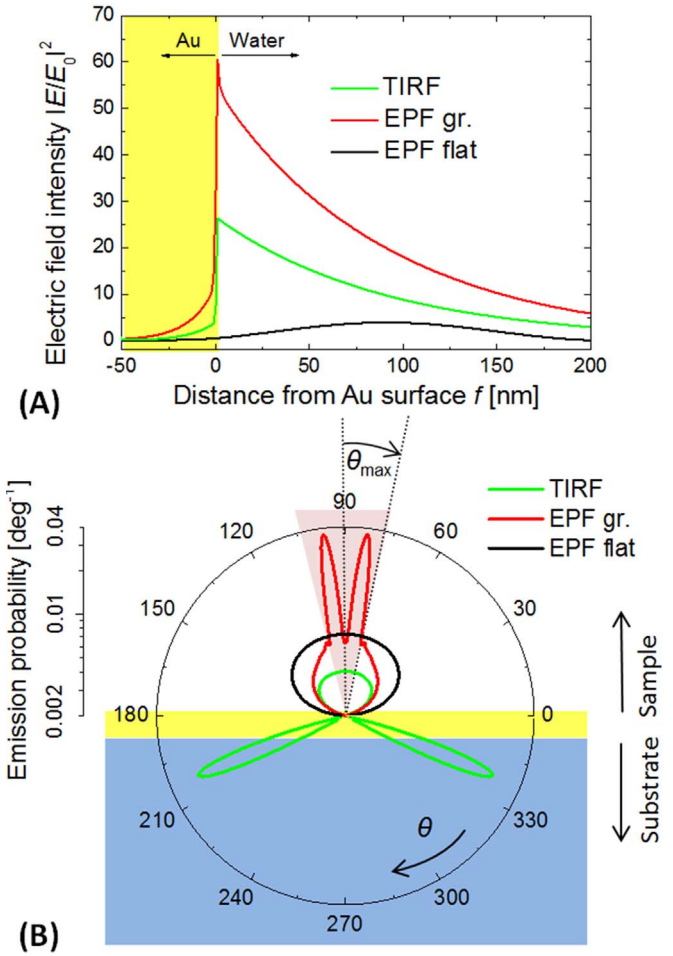


**Fig. 3.** A) Simulated electric field intensity upon the resonant excitation of SPs on a 50 nm thick gold film by Kretschmann geometry (green curve) used in TIRF geometry. Comparison with the field strength generated by diffraction coupling of normally incident beam to SPs on optically thick gold layer that is corrugated (red curve) and flat (black curve) used in EPF geometry. The electric intensity was normalized with that of the incident beam simulated for $\lambda_{ex}=633$ nm. B) Simulated dependence of emission probability on the polar angle θ averaged over the azimuthal angle Φ for ATR geometry (green curve) and EPF geometry with corrugated (red) and flat metal surface (black). (For interpretation of the references to color in this figure legend, the reader is referred to the web version of this article.)

## 3. Results and discussion

### 3.1. Simulations of plasmonic enhancement in TIRF and EPF configuration

In order to enhance the fluorescence signal *F* that is associated with molecular binding on the surface in heterogeneous assay, fluorophores that serve as labels can be exposed to the confined electromagnetic field of SPs. This enhancement originates mainly from two effects that are related to the interaction with SPs at emission $\lambda_{em}$ and excitation $\lambda_{ex}$ wavelengths of used fluorophores. First, the probing of the metallic sensor interface with resonantly excited SPs at $\lambda_{ex}$ allows to increase the excitation rate of fluorophores that is (far from saturation) proportional to the SP-enhanced electric field intensity $|E/E_0|^2$. Secondly, SPs travelling along the metallic surface at $\lambda_{em}$ provide an additional emission channel. The emission *via* SPs in conjunction with directional surface plasmon outcoupling allows to efficiently control angular distribution of emitted fluorescence light $F(\theta,\phi)$. By this means, the fraction of emitted photons *CE* that is extracted from the surface

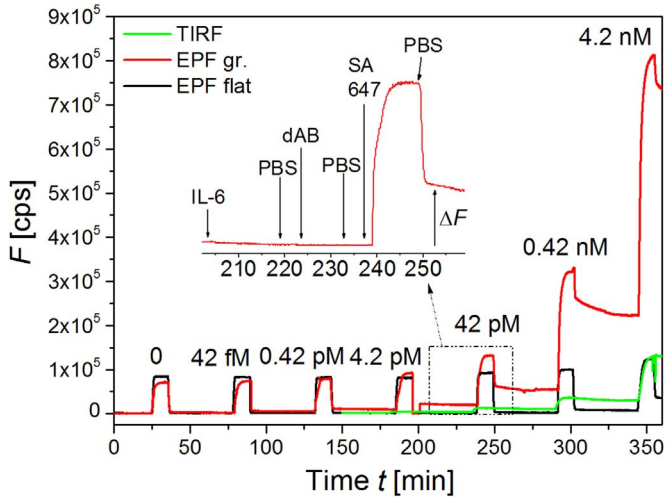


**Fig. 4.** Examples of the kinetics of fluorescence signal $F$ measured upon a series of assays with buffer samples spiked by IL-6 at concentrations of $4.2\times10^{-2}$–$4.2\times10^{3}$ pM. The kinetics data were measured by TIRF configuration with Kretschmann geometry (green curve), EPF configuration on a sensor chip with crossed diffraction grating (red curve), and reference EPF configuration on a flat gold substrate (black curve). (For interpretation of the references to color in this figure legend, the reader is referred to the web version of this article.)

and delivered to a detector can be substantially increased. Further on, the product of increased excitation rate at $\lambda_{ex}$ with the improved efficiency of extraction of emitted photonics at $\lambda_{em}$ is referred to as fluorescence enhancement factor *EF*. Two optical configurations were investigated by using an identical IL-6 assay, biointerface architecture, and flow cell geometry as depicted in Fig. 1. In the first configuration, total internal reflection fluorescence – TIRF – was used. The plasmonic amplification was utilized by the resonant excitation of SPs at $\lambda_{ex}$ which was implemented by using Kretschmann configuration of ATR method. The fluorescence signal emitted above the sensor chip through the transparent flow cell was detected. In the second epifluorescence – EPF – approach normally incident excitation beam at $\lambda_{ex}$ was resonantly coupled to SPs by first order diffraction on crossed grating [$p=\pm1$, $q=0$ in Eq. (2)]. The modulation profile of the crossed grating (described by using parameters $\alpha$ and $\beta$ defined above) was varied in simulations to achieve an optimum coupling efficiency (manifesting itself as a drop of reflectivity to zero at the resonance wavelength tuned to $\lambda_{ex}$), while keeping the full width half maximum (FWHM) of the resonance as narrow as possible. The fluorescence light that was emitted *via* SPs at $\lambda_{em}$ and subsequently out-coupled *via* the first order diffraction above the surface through attached flow-cell was detected.

Simulations presented in Fig. 3(A) compare the electric field intensity profile at $\lambda_{ex}$ for the investigated configurations. Upon the resonant excitation of SPs, the enhanced field intensity peaks at the gold interface and then exponentially decays into the adjacent aqueous medium for both Kretschmann and diffraction-based excitation. For the normally incident beam at a reference flat gold surface no plasmonic enhancement occurs and the profile of field intensity oscillates due to the interference of the incident and reflected beam. At the distance $f=20$ nm, the field reaches about $|E/E_0|^2=1.36$ for the reference structure. On the crossed diffraction grating, the diffraction coupling of normally incident beam to SPs provides the field intensity enhancement of $|E/E_0|^2=45$ at the distance from the gold surface of $f=20$ nm (averaged over the unit cell $\Lambda\times\Lambda$). For the Kretschmann geometry, lower field strength of $|E/E_0|^2=21$ is predicted at the same distance $f$. The reason is mainly the tilted angle of incidence $\theta_i$ under which the SPs are resonantly excited [for the simulated $\theta_i=51.5°$ the intensity enhancement roughly drops by a factor of $\cos(\theta_i)=0.62$].

Fluorophores excited above the gold surface emit photons at $\lambda_{em}$ directly into to the far field or *via* lossy waves that travel along the interface [23]. For the distance of $f=20$ nm, the majority of photons emitted at $\lambda_{em}\sim670$ nm are trapped by SPs above the gold surface. On the sensor chip that was developed for the EPF readout, these SPs can be partially diffraction out-coupled by the crossed grating structure into a directional beam propagating at polar angles between $\theta=0$–$12°$, see Fig. 3(B). This shaping of the emitted fluorescence intensity profile $F(\theta)$ translates to 6.1% of emitted photons propagating into the numerical aperture $NA=0.2$ of used optics. Contrary to that, on the optically thick flat gold surface the fluorescence intensity emitted *via* SPs is lost and it dissipates to heat due to the Ohmic losses. From the respective angular distribution of emitted fluorescence intensity $F(\theta)$ presented in Fig. 3(B) follows that only 1.4% of photons propagate to

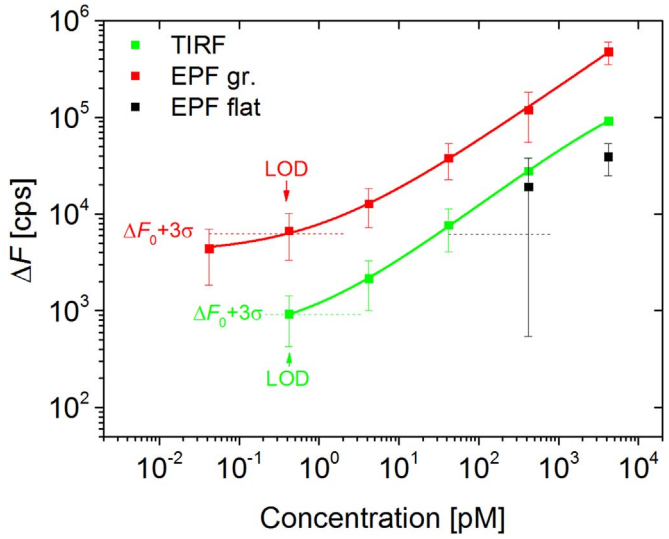


**Fig. 5.** Comparison of calibration curves for IL-6 assays with fluorescence readout by using TIRF with Kretschmann geometry (green squares), EPF on a crossed gold grating (red squares), and reference flat gold surface (black squares). The measured data were fitted by logistic sigmoidal function (lines) and error bars show standard deviation σ. (For interpretation of the references to color in this figure legend, the reader is referred to the web version of this article.)

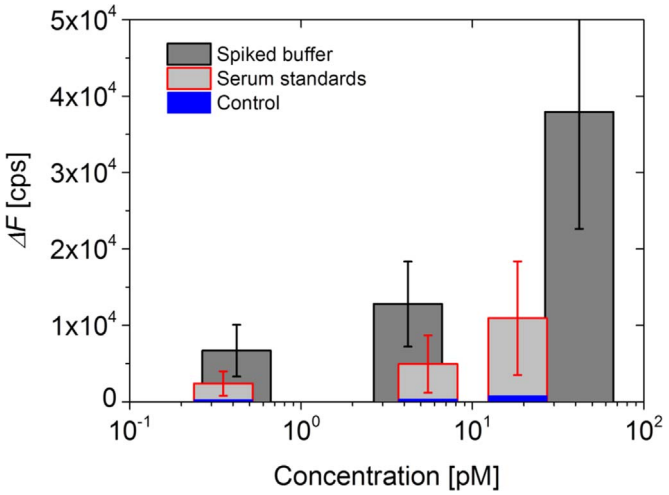


**Fig. 6.** Plasmonically amplified assay of standard serum samples (diluted with 1:10 with working buffer) on a chip functionalized with specific anti-IL-6 antibodies (dark gray columns) and reference anti-p53 antibodies (blue columns). The response is compared to that for series of buffer samples spiked with IL-6. EPF readout with a grating sensor chip was used. (For interpretation of the references to color in this figure legend, the reader is referred to the web version of this article.)

the $NA=0.2$. When the thickness of the flat metal film on a glass substrate is decreased to 50 nm, the SPs generated at $\lambda_{em}$ are back coupled to waves travelling into the substrate by reverse Kretschmann configuration. However, such out-coupling does not provide improved collection efficiency in the readout used in this work (see Fig. 1(B)) as the fluorescence is preferably re-emitted in the opposite direction to the collecting optics. For this geometry, only 0.82% of emitted photons can reach the detector when a lens with $NA=0.2$ is used.

In summary, the presented simulations predict that the plasmonic amplification based on the Kretschmann configuration offers moderate enhancement factor of $EF=7.4$ as it only takes advantage of the SP-enhanced excitation rate at $\lambda_{ex}$. Using crossed grating structures for diffraction-coupling to SPs offers the means to exploit both SP-enhanced excitation at $\lambda_{ex}$ and SP-coupled directional fluorescence emission at $\lambda_{em}$. This translates to the higher predicted enhancement factor of $EF=96$ when compared to EPF readout on a flat metal film. It should be noted that these values were obtained by averaging of $|E/E_0|^2 \times CE$ for all possible orientations of emitters as described in more detail in our previous work [13,24]. Therefore, the predicted enhancement values differ from a simple product of $|E/E_0|^2$ and $CE$ calculated above.

### 3.2. Application to fluorescence IL-6 immunoassay

The performance of TIRF and EPF sensors with plasmonic amplification of fluorescence signal was experimentally evaluated for IL-6 sandwich immunoassay. Fig. 4 shows an example of the fluorescence intensity kinetics that was measured upon sequential analysis of samples with IL-6 concentration of 0, $4.2 \times 10^{-2}$, 0.42, 4.2, 42, $4.2 \times 10^2$ and $4.2 \times 10^3$ pM (these samples were prepared by spiking the working buffer with purified IL-6). As indicated in the inset of Fig. 4, each sample was flowed for 15 min in order to capture the target analyte at the surface carrying specific cAb. Then the surface was subsequently reacted with dAb-biotin conjugate and with streptavidin labeled with Alexa Fluor 647 dye (SA). Fig. 4 shows that the fluorescence signal $F$ abruptly jumps after the injecting of SA due to the excitation of fluorophores in the bulk solution. Then, the fluorescence signal $F$ gradually increases due to the affinity binding of SA until it reaches saturation. After a rinsing, fluorescence signal $F$ rapidly drops down to a level that is higher than that prior to the injecting of SA. This fluorescence difference $\Delta F$ is attributed to the specific binding of SA to the sandwich formed at the surface by the affinity interaction between cAb, IL-6, and dAb. It is worth mentioning that the fluorescence signal change originating from the bulk was much stronger than the response $\Delta F$ associated with the specific binding (EPF readout on a flat gold surface represented by black curve in Fig. 4) which complicates real-time *in situ* observation of surface reactions. Plasmonic amplification based on the probing by confined SP field allows increasing the surface fluorescence intensity $\Delta F$ and makes it substantially stronger than the background bulk signal. This effect is apparent from data presented in Fig. 4 for EPF readout geometry with crossed diffraction grating (red curve) as well as for TIRF geometry exploiting Kretschmann configuration (green curve). For the concentration of target analyte of 4.2 nM, the increase in the fluorescence intensity $\Delta F$ measured by EPF on crossed grating gold surface was about 17-fold higher than that observed on a reference flat surface. For the TIRF readout with plasmonic amplification, the fluorescence signal was 4 times higher than the reference measurement. Both these enhancement factors are significantly lower than those predicted by simulations. The enhancement factor for crossed rating EPF is about 6-fold smaller than the one predicted by simulations ($EF=96$) and experimentally measured in our previous work [13]. For the TIRF readout, the fluorescence increase is about 1.8-times lower than the theory suggests. These deviations can be partially attributed to the model that does not take into account additional effects related to *e.g.* roughness and to deviations of the prepared structures from the optimum ones that were simulated. Particularly, possible detuning of SPR resonance due to the functionalization of the sensor surface with capture antibody cAb can lead to the variations from the optimum parameters.

The sensor response $\Delta F$ was measured in triplicate for each concentration by using the plasmonically amplified EPF and TIRF readout as well as for the reference geometry. As seen in Fig. 5, calibration curves were established and there was determined the background signal $\Delta F_0$ and standard deviation of the blank measurement $\sigma$ that takes into account the dark current from photomultiplier, stray light intensity associated with the scattering of the beam at the excitation wavelength, and unspecific sorption of SA to the sensor surface. The average background signal of $\Delta F_0=2.0 \times 10^3$ cps was observed for the EPF readout with the crossed gold grating. On a reference flat gold surface, lower background of $\Delta F_0=1.0 \times 10^3$ cps was measured due to the lower signal from unspecifically adsorbed molecules to the gold surface. For the TIRF geometry, background signal of $\Delta F_0=0.8 \times 10^3$ was observed and it can be attributed to the fact that the excitation beam travelled on the opposite side of the optics that was used for collecting of fluorescence light. The lowest standard deviation of the background signal was $\sigma=0.033 \times 10^3$ cps for the TIRF configuration. On a flat gold surface with EPF readout there was measured $\sigma=0.25 \times 10^3$ and on the grating surface $\sigma=1.3 \times 10^3$ cps. From the established calibration curves in Fig. 5, the limit of detection (LOD) was determined as the concentration where the fitted sigmoidal function intersects with the value $\Delta F_0 + 3\sigma$. Interestingly, the limit of detection for both plasmonically amplified EPF and TIRF readout of IL-6 assay yields the same value 0.4 pM (for the reference flat gold surface and EPF readout the LOD was not determined due to the large error and weak fluorescence response). This result data illustrates that the advantage of higher plasmonic enhancement of fluorescence signal for the EPF geometry is compensated by the lower background signal that was observed for TIRF configuration.

Finally, the EPF sensor with crossed grating was tested for the analysis of standard serum samples with IL-6. In this experiment two sets of crossed grating chips were prepared and functionalized either with anti-IL-6 antibodies against the target analyte or with a reference antibody against p53. On these sensor chips, IL-6 assay was performed with standard serum samples at concentration of 0.35, 5.5, and 18 pM that were diluted 1:10 with a working buffer. The assay was measured in triplicate for each sample and the specific, as well as the control response, is showed in Fig. 6. For the testing of serum samples, the sensor response $\Delta F$ was determined as a difference between the fluorescence signal before and after incubation of the sensor surface with SA. The obtained results reveal that for all analyzed samples there was possible distinguishing the response on the specific sensor chip from that on the reference chip.

## 4. Conclusions

The performance of sandwich immunoassay with plasmonically-amplified fluorescence readout is compared for the readout geometry utilizing epifluorescence – EPF – and total internal reflection fluorescence – TIRF. It employs resonant excitation of propagating surface plasmons by using crossed diffraction grating and Kretschmann configuration of attenuated total reflection method. The probing of the assay on a continuous gold film by propagating surface plasmons improves the limit of detection by selective enhancement of fluorescence intensity emitted from the

close proximity to the surface. The TIRF geometry provides a moderate enhancement of detected signal, however, offers the advantage of low background. For an IL-6 assay both configurations offered a limit of detection of 0.4 pM for 15 min reaction of a sample with a surface comparable to other assays reported for surface plasmon-enhanced fluorescence with Kretschmann geometry [25,26].

In addition, TIRF as well as EPF selectively increased the fluorescence signal on the surface which enables measuring kinetics of surface reaction by efficient suppressing of background signal originating from the bulk. The developed EPF sensor with plasmonic amplification utilizing crossed gratings sensor chip was demonstrated for the analysis of serum samples with IL-6 concentrations below pM which can find its applications in rapid detection of this inflammation biomarker.

IL-6 levels in human serum can vary from sub-pM levels in healthy individuals, elevated levels in *e.g.* cancer [27,28] to concentrations exceeding 50 pM upon sepsis [29,30]. The demonstrated plasmonically amplified readout of fluorescence sandwich immunoassay would allow discriminating such cases based on the analysis of serum. It should be mentioned that the limit of detection of the presented instrument is still above that achieved by ELISA method [31] and it would not be suitable for quantitative discrimination of IL-6 concentrations in serum of healthy individuals. However, the presented implementations of plasmonically enhanced fluorescence may offer substantially faster detection time (40 min compared to several hours) which can be further shortened by using directly labeled detection antibodies. In addition, large binding capacity interface architectures [32] and probing with more confined plasmonic modes [24] can be utilized in order to reach stronger enhancement of the fluorescence signal and lower limit of detection.

## Acknowledgments

This project has received funding from the European Union's Horizon 2020 Research and Innovation Programme under Grant agreement No. 633937, project ULTRAPLACAD, and FEMTECH – Frauen in Forschung und Technologie Initiative of the Austrian Ministry for Transportation, Innovation and Technology.

## References

[1] M. Bally, M. Halter, J. Voros, H.M. Grandin, Optical microarray biosensing techniques, Surf. Interface Anal. 38 (11) (2006) 1442–1458.
[2] M. Seidel, R. Niessner, Automated analytical microarrays: a critical review, Anal. Bioanal. Chem. 391 (5) (2008) 1521–1544.
[3] E. Fort, S. Gresillon, Surface enhanced fluorescence, J. Phys. D: Appl. Phys. 41 (1) (2008).
[4] S. Lal, N.K. Grady, J. Kundu, C.S. Levin, J.B. Lassiter, N.J. Halas, Tailoring plasmonic substrates for surface enhanced spectroscopies, Chem. Soc. Rev. 37 (5) (2008) 898–911.
[5] B. Sharma, R.R. Frontiera, A.I. Henry, E. Ringe, R.P. Van Duyne, SERS : materials, applications, and the future, Mater. Today 15 (1–2) (2012) 16–25.
[6] C. Hoppener, L. Novotny, Exploiting the light-metal interaction for biomolecular sensing and imaging, Q. Rev. Biophys. 45 (2) (2012) 209–255.
[7] M. Bauch, K. Toma, M. Toma, Q. Zhang, J. Dostalek, Plasmon-enhanced fluorescence biosensors: a review, Plasmonics 9 (4) (2014) 1–19.
[8] J.R. Lakowicz, J. Malicka, I. Gryczynski, Z. Gryczynski, Directional surface plasmon-coupled emission: a new method for high sensitivity detection, Biochem. Biophys. Res. Commun. 307 (3) (2003) 435–439.
[9] M.E. Stewart, C.R. Anderton, L.B. Thompson, J. Maria, S.K. Gray, J.A. Rogers, R. G. Nuzzo, Nanostructured plasmonic sensors, Chem. Rev. 108 (2) (2008) 494–521.
[10] J.W. Attridge, P.B. Daniels, J.K. Deacon, G.A. Robinson, G.P. Davidson, Sensitivity enhancement of optical Immunosensors by the use of a surface-plasmon resonance fluoroimmunoassay, Biosens. Bioelectron. 6 (3) (1991) 201–214.
[11] T. Liebermann, W. Knoll, Surface-plasmon field-enhanced fluorescence spectroscopy, Coll. Surf. A: Physicochem. Eng. Asp. 171 (1–3) (2000) 115–130.
[12] K. Toma, P. Adam, M. Vala, J. Homola, W. Knoll, J. Dostalek, Compact biochip for plasmon-enhanced fluorescence biosensor, Opt. Express 21 (8) (2013) 10121–10132.
[13] M. Bauch, S. Hageneder, J. Dostalek, Plasmonic amplification for bioassays with epi-fluorescence readout, Opt. Express 22 (26) (2014) 32026–32038.
[14] K. Tawa, X.Q. Cui, K. Kintaka, J. Nishii, K. Morigaki, Sensitive bioimaging in microfluidic channels on the plasmonic substrate: application of an enhanced fluorescence based on the reverse coupling mode, J. Photochem. Photobiol. A: Chem. 221 (2–3) (2011) 261–267.
[15] M. Lukaszewicz, B. Mroczko, M. Szmitkowski, Clinical significance of interleukin-6 (IL-6) as a prognostic factor of cancer disease, Pol. Arch. Med Wewn. 117 (5–6) (2007) 247–251.
[16] D.S. Hong, L.S. Angelo, R. Kurzrock, Interleukin-6 and its receptor in cancer, Cancer 110 (9) (2007) 1911–1928.
[17] M. Helle, L. Boeije, E. de Groot, A. de Vos, L. Aarden, Sensitive ELISA for interleukin-6, J. Immun. Methods 138 (1) (1991) 47–56.
[18] H. Chen, T.K. Choo, J. Huang, Y. Wang, Y. Liu, M. Platt, A. Palaniappan, B. Liedberg, A.I.Y. Tok, Label-free electronic detection of interleukin-6 using horizontally aligned carbon nanotubes, Mater. Des. 90 (2016) 852–857.
[19] T. Li, M. Yang, Electrochemical sensor utilizing ferrocene loaded porous polyelectrolyte nanoparticles as label for the detection of protein biomarker IL-6, Sens. Actuators B 158 (1) (2011) 361–365.
[20] S. Krishnamoorthy, A.A. Iliadis, T. Bei, G.P. Chrousos, An interleukin-6 ZnO/SiO2/Si surface acoustic wave biosensor, Biosens. Bioelectron. 24 (2) (2008) 313–318.
[21] R. Kapoor, C.-W. Wang, Highly specific detection of interleukin-6 (IL-6) protein using combination tapered fiber-optic biosensor dip-probe, Biosens. Bioelectron. 24 (8) (2009) 2696–2701.
[22] P. Buchegger, C. Preininger, Four assay designs and on-chip calibration: gadgets for a sepsis protein array, Anal. Chem. 86 (6) (2014) 3174–3180.
[23] G.W. Ford, W.H. Weber, Electromagnetic interactions of molecules with metal surfaces, Phys. Rep. 113 (4) (1984) 195–287.
[24] M. Bauch, J. Dostalek, Collective localized surface plasmons for high performance fluorescence biosensing, Opt. Express 21 (17) (2013) 20470–20483.
[25] Y. Wang, J. Dostalek, W. Knoll, Biosensor for detection of aflatoxin $M_1$ in milk based on long range surface plasmon enhanced fluorescence spectroscopy, Biosens. Bioelectron. 24 (7) (2009) 2264–2267.
[26] M.L.M. Vareiro, J. Liu, W. Knoll, K. Zak, D. Williams, A.T.A. Jenkins, Surface plasmon fluorescence measurements of human chorionic gonadotrophin: Role of antibody orientation in obtaining enhanced sensitivity and limit of detection, Anal. Chem. 77 (8) (2005) 2426–2431.
[27] O. Arican, M. Aral, S. Sasmaz, P. Ciragil, Serum levels of TNF-alpha, IFN-beta, IL-6, IL-8, Mediat. Inflamm. 2005 (5) (2005) 273–279.
[28] T. Robak, A. Wierzbowska, M. Blasinska-Morawiec, A. Korycka, J.Z. Blonski, Serum levels of IL-6 type cytokines and soluble IL-6 receptors in active B-cell chronic lymphocytic leukemia and in cladribine induced remission, Mediat. Inflamm. 8 (6) (1999).
[29] D.W. Jekarl, S.-Y. Lee, J. Lee, Y.-J. Park, Y. Kim, J.H. Park, J.H. Wee, S.P. Choi, Procalcitonin as a diagnostic marker and IL-6 as a prognostic marker for sepsis, Diagn. Microbiol. Infect. Dis. 75 (4) (2013) 342–347.
[30] S. Harbarth, K. Holeckova, C. Froidevaux, D. Pittet, B. Ricou, G.E. Grau, L. Vadas, J. Pugin, Diagnostic value of procalcitonin, interleukin-6, and interleukin-8 in critically Ill patients admitted with suspected sepsis, Am. J. Resp. Crit. Care Med. 164 (3) (2001) 396–402.
[31] I. R&D Systems, ⟨https://www.rndsystems.com/products/human-il-6-quantikine-hs-elisa-kit_hs600b#product-details⟩, 2016 (accessed 18.04.16).
[32] Y. Wang, A. Brunsen, U. Jonas, J. Dostalek, W. Knoll, Prostate specific antigen biosensor based on long range surface plasmon-enhanced fluorescence spectroscopy and dextran hydrogel binding matrix, Anal. Chem. 81 (23) (2009) 9625–9632.